nature biotechnology

Magnetic resonance tracking of dendritic cells in melanoma patients for monitoring of cellular therapy

I Jolanda M de Vries[1,2], W Joost Lesterhuis[3], Jelle O Barentsz[4], Pauline Verdijk[1], J Han van Krieken[5], Otto C Boerman[6], Wim J G Oyen[6], Johannes J Bonenkamp[7], Jan B Boezeman[8], Gosse J Adema[1], Jeff W M Bulte[9], Tom W J Scheenen[4], Cornelis J A Punt[3], Arend Heerschap[4] & Carl G Figdor[1]

The success of cellular therapies will depend in part on accurate delivery of cells to target organs. In dendritic cell therapy, in particular, delivery and subsequent migration of cells to regional lymph nodes is essential for effective stimulation of the immune system. We show here that *in vivo* magnetic resonance tracking of magnetically labeled cells is feasible in humans for detecting very low numbers of dendritic cells in conjunction with detailed anatomical information. Autologous dendritic cells were labeled with a clinical superparamagnetic iron oxide formulation or ^{111}In-oxine and were co-injected intranodally in melanoma patients under ultrasound guidance. In contrast to scintigraphic imaging, magnetic resonance imaging (MRI) allowed assessment of the accuracy of dendritic cell delivery and of inter- and intra-nodal cell migration patterns. MRI cell tracking using iron oxides appears clinically safe and well suited to monitor cellular therapy in humans.

Cellular therapies using stem cells and immune cells are being increasingly applied in clinical trials. Accurate delivery of cells to target organs can make the difference between failure or success. Because of their pivotal role in initiating an immune response, dendritic cells are of widespread interest as a means of enhancing the endogenous immune response against tumor cells. Tumor antigen–loaded dendritic cell vaccines have been introduced in the clinic and have proven feasible and nontoxic, and both immunological and clinical responses have been observed[1]. However, effective immune induction is limited to a minority of patients. One possible explanation of this is insufficient delivery of dendritic cells to the target organs.

For effective immunotherapy, dendritic cells must migrate throughout the vascular and lymphatic system to present their antigens to T cells located within lymph nodes. In independent studies, dendritic cells have been administered by different routes: intradermally, subcutaneously, intravenously or using combinations of these routes. Alternatively, dendritic cells can be injected directly into the lymph node[2]. Thus far it has not been clear which route of administration is optimal. The design of optimal dendritic cell therapy would therefore be facilitated by technologies for monitoring dendritic cell trafficking. Dendritic cells have previously been labeled with radionuclides for scintigraphic imaging, which is the only clinical cellular imaging modality approved by the US Food and Drug Administration (FDA)[3–5]. A major drawback of scintigraphy, however, is the lack of anatomical detail; it allows only gross anatomical determination of migration between lymph nodes without the ability to assess the intranodal distribution pattern of dendritic cells within each lymph node. Furthermore, accurate cell delivery, which may be essential for subsequent migration into nearby lymph nodes, cannot be properly evaluated owing to scintigraphy's lack of spatial resolution.

In contrast, MRI is well suited to obtain three-dimensional, whole-body, high-resolution images and is widely used in clinical practice. The most sensitive existing markers to label cells for magnetic resonance detection are (ultrasmall) superparamagnetic iron oxide ((U)SPIO) particles[6]. Initially applied as a marker for cells of the reticulo-endothelial system, including the liver[7] and lymph nodes[8], these contrast agents are now either FDA-approved as a liver agent (SPIO; Feridex-USA; Endorem-Europe) or in late-phase clinical trials as a lymph node agent (USPIO; Combidex-USA; Sinerem-Europe)[9]. They are nontoxic and biodegradable[10]. Recently, SPIO particles have been applied as a magnetic label to detect cells after local grafting[11–14] or systemic injection[15–18], including dendritic cells labeled with a nonclinical-grade SPIO preparation through a two-step monoclonal antibody approach[19]. These studies have all been performed in animal models. Translation of these techniques from animal models to humans is not straightforward because SPIO-labeling raises safety concerns associated with the use in patients of adjunct compounds, such as transfection agents.

In this study, we obviated these concerns by taking advantage of the fact that immature dendritic cells naturally endocytose clinically applied, FDA-approved SPIO-labels in substantial amounts. We found that cells could be labeled with high efficiency without affecting their function. We then investigated the biodistribution of SPIO-labeled dendritic cells applied as cancer vaccines in melanoma patients

Departments of [1]Tumor Immunology, [2]Pediatric Oncology, [3]Medical Oncology, [4]Radiology, [5]Pathology, [6]Nuclear Medicine, [7]Surgery and [8]Central Hematological Laboratory, Radboud University Nijmegen Medical Center and Nijmegen Center for Molecular Life Sciences, Geert Grooteplein 28, 6500 HB Nijmegen, The Netherlands, [9]The Russell H. Morgan Department of Radiology and Radiological Science, Division of MR Research, and Institute for Cell Engineering, Johns Hopkins University School of Medicine, 217 Traylor, 720 Rutland Ave., Baltimore, Maryland 21205, USA. Correspondence should be addressed to C.G.F. (c.figdor@ncmls.ru.nl) or J.W.M.B. (jwmbulte@mri.jhu.edu).

Received 12 April; accepted 25 August; published online 30 October 2005; doi:10.1038/nbt1154

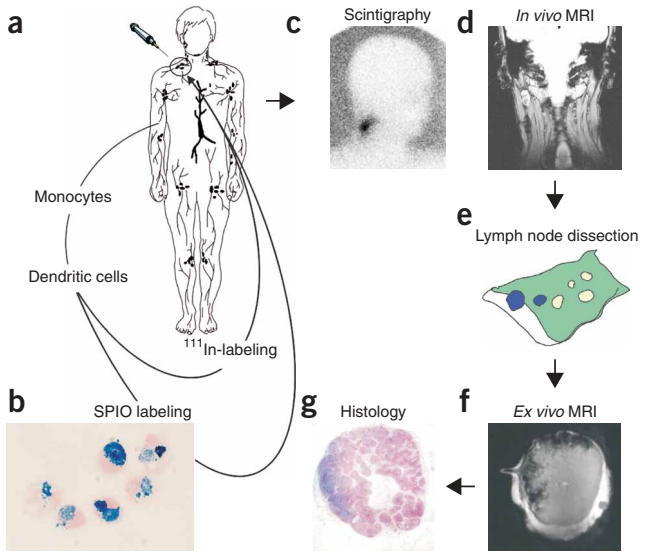

Figure 1 Study protocol. (**a**) Monocytes are obtained by cytopheresis from stage-III melanoma patients. (**b**) They are cultured and labeled with SPIO particles and ^{111}In. (**c**,**d**) The cells are then injected intranodally into a (either cervical, inguinal or axillary) lymph node basin that is to be resected and their biodistribution is monitored *in vivo* by scintigraphy (**c**) and MRI at 3 Tesla (**d**). (**e**–**g**) The lymph node basis is resected and separate lymph nodes are visualized with high resolution MRI at 7 Tesla (**f**) and histology (**g**).

using MRI. *In vitro*-generated dendritic cells loaded with tumor-derived antigenic peptides were administered to stage-III melanoma patients as outlined in **Figure 1** (refs. 3,20). Dendritic cells were labeled with ^{111}In-oxine and SPIO (Endorem) separately and co-injected in a lymph node in the lymph node basin to be resected. This provided a unique opportunity not only to obtain magnetic resonance scans at 3 Tesla (T) before surgery, but also to generate high-resolution magnetic resonance images at 7 T of individual resected lymph nodes and to correlate the results with scintigraphy and (immuno)histopathology (**Fig. 1**). We show that magnetic resonance tracking of magnetically labeled cells is a clinically safe procedure that, because of its high resolution and excellent soft tissue contrast, appears ideally suited to monitor novel experimental cell therapies in patients.

RESULTS

In vivo MRI and scintigraphy of dendritic cells

We loaded dendritic cells with SPIO particles by coculturing immature dendritic cells with 200 μg/ml SPIO, as immature but not mature dendritic cells are highly phagocytic[21]. Several tests were conducted to determine whether the labeling procedure affected the cells' viability or function. First, we confirmed that all cells had taken up a substantial amount of SPIO by the end of the culture period (**Fig. 1b**). Second, the phenotypes of SPIO-labeled and unlabeled cells appeared similar (**Fig. 2a**). Third, the random migration on fibronectin-coated wells[3] showed that SPIO-labeled dendritic cells migrated as well as unlabeled- or ^{111}In-labeled cells (**Fig. 2b**). Finally, SPIO-labeling of dendritic cells loaded with the melanoma-specific peptide gp100:154-162 was found not to affect the peptide-specific production of interferon-γ by a gp100:154-162-specific T-cell line[22] (**Fig. 2c**), indicating that the antigen-presentation function of dendritic cells remained unaffected after labeling. Together these results demonstrate that SPIO labeling does not affect the cells' phenotype or function.

Eight stage-III melanoma patients received an intranodal injection under ultrasound guidance of a mixture of ^{111}In- and SPIO-labeled dendritic cells (ratio 1:1) 2 d before radical dissection of regional lymph nodes. Patients were imaged before and 2 d after the injection by both scintigraphic imaging and MRI to monitor delivery of the dendritic cells and their subsequent migration to nearby lymph nodes. Scintigraphic imaging confirmed and extended previous findings that although a significant percentage of dendritic cells remained at the injection site, some did migrate to nearby lymph nodes. In four of eight patients, 1% to 40% of total ^{111}In activity was found in regional lymph nodes draining the injected lymph node, indicating migration of ^{111}In-labeled dendritic cells (**Fig. 3d**, **Table 1** and **Supplementary Fig. 1** online).

The scintigraphic images were compared with *in vivo* magnetic resonance images obtained on a 3-T magnetic resonance system (**Fig. 3**). Comparison of gradient echo images before and after cell injection (**Fig. 3a**,**c**; patient 1) showed that the injected SPIO-labeled dendritic cells resulted in a significant decrease in signal intensity at the injection site. After injection, turbo spin echo (SE) images, which are relatively insensitive to SPIO-induced magnetic susceptibility effects, were also obtained (**Fig. 3b**). By comparing the iron-insensitive magnetic resonance spin echo sequence with iron-sensitive gradient echo sequences, one can reliably detect the presence of iron in a lymph node[9].

In SE images, lymph nodes generally appear as dark-gray structures. In gradient echo images, they are white (compare open arrows in **Fig. 3e**,**f**; **k**,**l** and **m**,**n**; patient 3); a large decrease in signal intensity at the sites of the lymph nodes indicated the presence of SPIO-labeled cells (closed arrows in **Fig. 3**). ^{111}In- and SPIO-labeled cells co-localized in the same areas, proving that the locations detected by MRI indeed represent injected and migrated dendritic cells (**Fig. 3e**–**n**). All lymph nodes that showed ^{111}In activity were also

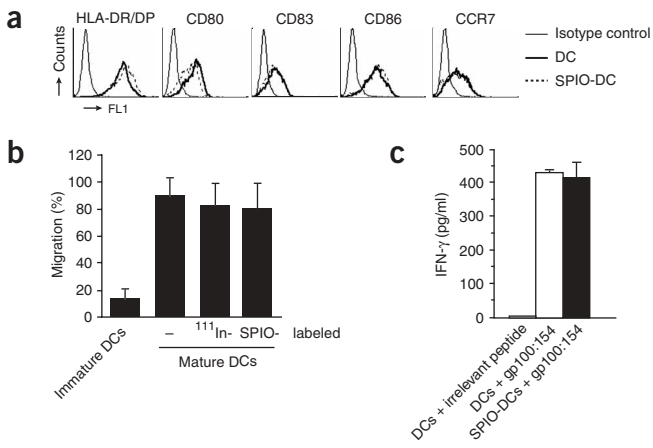

Figure 2 Phenotypical and functional characterization of SPIO-labeled dendritic cells. (**a**) FACS analysis of the expression of major histocompatibility complex class II (HLA-DR/DP) and costimulatory (CD80 and CD86) molecules, dendritic cell maturation marker CD83 and chemokine receptor CCR7. (**b**) Migratory capacity of dendritic cells determined by the percentage of dendritic cells labeled with or without SPIO or ^{111}In that migrate on a fibronectin surface in a random *in vitro* migration assay. (**c**) Interferon-γ production by gp100:154-162-specific T-cell line cocultured with unlabeled, gp100:154-162-loaded dendritic cell, SPIO-labeled, gp100:154-162-loaded dendritic cells or unlabeled dendritic cells loaded with an irrelevant peptide.

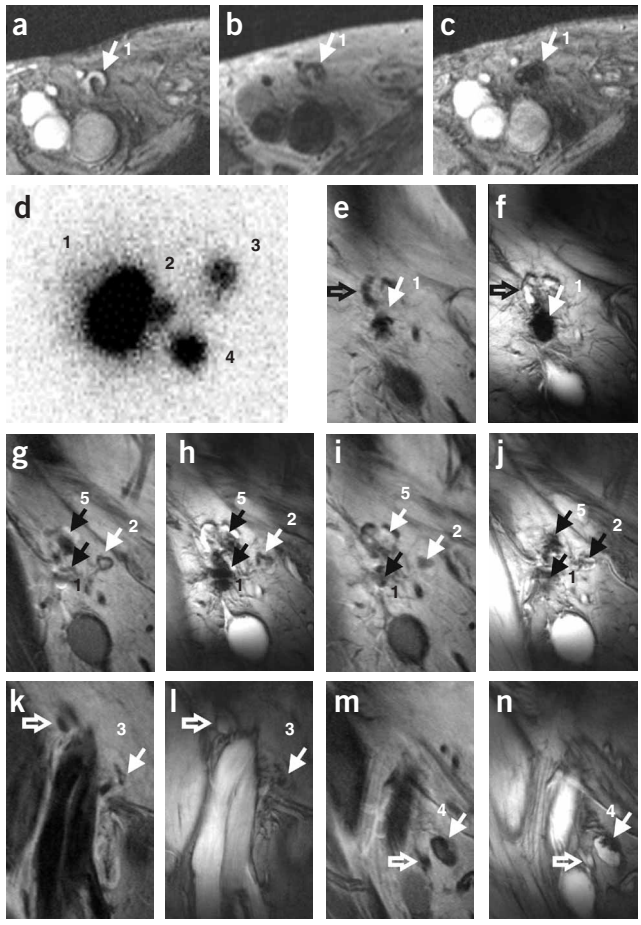

Figure 3 *In vivo* scintigraphic and MRI. (**a–c**) Monitoring of the delivery of dendritic cells labeled with SPIO and ^{111}In by MRI before and after intranodal injection in patient 1. (**a**) Gradient echo transversal magnetic resonance image before vaccination showing a right inguinal lymph node with a hyperintense signal area (1). (**b**) SE (technique much less sensitive for SPIO) transverse magnetic resonance image obtained from the same lymph node after vaccination. (**c**) Gradient echo transverse magnetic resonance images after vaccination in same position as **b** showing a decreased signal intensity of lymph node 1. (**d–n**) Monitoring of *in vivo* migration of SPIO and ^{111}In-labeled dendritic cells with MRI and scintigraphy after injection in a right inguinal lymph node in patient 3. (**d**) *In vivo* scintigraphy 2 d after vaccination showing migration of the dendritic cells from the injection lymph node (1) to three following lymph nodes (2–4). (**e–n**) Five image pairs of a coronal gradient echo and SE image 2 d after vaccination showing migration of the dendritic cells from the injection lymph node 1 (**e** and **f**) to four following lymph nodes (**g–n**). Open arrows indicate lymph nodes that do not contain SPIO, on the SE images these nodes are dark-gray; on gradient echo images they are white. Closed arrows indicate lymph nodes that are positive for SPIO in the gradient echo magnetic resonance image. On gradient echo images SPIO-containing lymph nodes have a decreased signal intensity compared to SE images. The concentration of SPIO in lymph node 1 was very high, resulting even in a decreased signal intensity in the SE image. The lymph node that was identified by the scintigraphy as the injection lymph node (lymph node 1 in **d**) actually consisted of two distinct lymph nodes as evidenced by MRI (lymph nodes 1 and 5).

positive in MRI. However, because MRI has a higher spatial resolution, the MRI images revealed more lymph nodes containing migrated dendritic cells as compared with the scintigraphic images (**Table 1**). In addition, scintigraphic imaging saturates the image such that multiple adjacent lymph nodes may appear as one. An example is shown in **Figure 3**. In patient 3, four positive lymph nodes were identified by scintigraphy. However, the magnetic resonance images revealed five lymph nodes, as the hot spot of lymph node 1 actually consisted of two separate lymph nodes, with the second one lying close to the injection node (**Fig. 3d**,**g**,**h** and **Supplementary Video 1** online).

From the scintigraphy of the resected lymph node basin from patient 1, we could calculate that 2% of 7.5×10^6 dendritic cells migrated to draining lymph node number 4 (see **Supplementary Fig. 1** online). This particular node was also visible by MRI, indicating that as few as 1.5×10^5 migrated cells could readily be visualized. The node had a volume of $2.3 \times 7.6 \times 3.5$ mm (90 voxels in one slice).

Table 1 Comparing scintigraphy and MRI for monitoring of cell migration

Patient	Injection site	Injection correctly in LN	Number of LNs visualized on *in vivo* scintigraphy[a]	Number of LNs visualized on *ex vivo* scintigraphy[a]	Number of LNs visualized on MR[a]
1	Inguinal LN	Yes	2 (4%)	4 (40%)	4
2	Inguinal LN	Yes	1 (0%)	2 (1%)	3
3 Right	Inguinal LN	Yes	4 (4.2%)	5 (n.d.)	5
Left	Inguinal LN	Yes	2 (1.7%)	n.d.	2
4	Cervical LN	Partly[b]	2 (17%)	2 (n.d.)	2
5	Axillary LN	No	1 (0%)	1 (0%)	0[c]
6	Auxiliary LN	Partly[b]	1 (0%)	1 (0%)	1
7	Inguinal LN	No	1 (0%)	1 (0%)	0[c]
8	Inguinal LN	No	1 (0%)	1 (0%)	0[c]

[a]Including the injected LN, between brackets the total percentage of ^{111}In-activity at the site(s) distant from the injection depot is given (only for scintigraphy).
[b]Part of the cells were injected outside the LN, mostly in the perinodal tissue. [c]SPIO was detected only outside the LN. LN, lymph node.

Assuming that the distribution of SPIO-positive cells in the lymph node was homogeneous, as a rough estimate $\sim 2 \times 10^3$ cells/voxel could be visualized. Because the distribution is inhomogeneous, the actual value may be larger. Notably, the additional anatomical information provided by the magnetic resonance images could confirm that the injected dendritic cells were truly localized within the lymph node. In addition, MRI demonstrated that in three patients the dendritic cells were actually delivered not into the lymph node but in the perinodular fat (**Fig. 4a**,**b**). Notably, in all three patients no dendritic cell migration to draining lymph nodes was observed (**Table 1**). Furthermore, in two patients, dendritic cells were injected only partly in the target lymph node and migration of dendritic cells was registered in only one of them. The total number of SPIO-positive dendritic cells imaged by magnetic resonance was significantly correlated with the success of the intranodal injection (see **Supplementary Fig. 2**, $P < 0.05$). Thus, in contrast to MRI, which allows verification that hotspots are actually lymph nodes, scintigraphy cannot distinguish between correct and incorrect intranodal injections, leading to erroneous classification of injection sites as lymph nodes.

Analysis of the number of cases in which one technique was more accurate in imaging true dendritic cell–positive lymph nodes showed that MRI was significantly better than scintigraphy ($P < 0.05$). Thus, the detailed anatomical information (combination of high spatial resolution and excellent soft tissue contrast) of MRI is a clear advantage compared with scintigraphic imaging, allowing both verification of accurate delivery and monitoring of subsequent migration of SPIO-labeled cells.

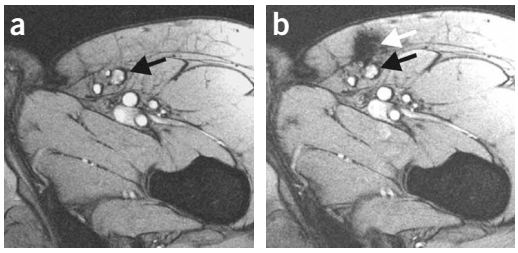

Figure 4 Monitoring of the accuracy of delivery of SPIO-labeled cells using MRI. (**a**) MRI before vaccination; the inguinal lymph node to be injected is indicated with a black arrow. (**b**) MRI after injection showing that the dendritic cells were not accurately delivered into the inguinal lymph node (black arrow) but in the vicinity, in the subcutaneous fat (white arrow).

Ex vivo MRI and histology of resected lymph nodes

As the melanoma patients were scheduled for regional lymph node dissection, a unique opportunity existed to investigate the biodistribution of the injected dendritic cells in more detail in individual resected lymph nodes by high-resolution MRI at 7 T (**Fig. 5a**,**c**). All lymph nodes that contained ^{111}In-positive dendritic cells as determined by a gamma probe were also positive for SPIO-labeled cells, validating the ability of MRI to detect and localize low numbers of injected and migrated SPIO-labeled cells. As expected when SPIO-labeled cells are present, the gradient echo images of these nodes showed much larger areas in the lymph nodes that are hypointense as compared with the SE images (see **Supplementary Videos 2** and **3** online).

Localization of SPIO-labeled dendritic cells in the lymph nodes was further confirmed by histology after Prussian blue staining of lymph node sections (**Fig. 5b**,**d**). There was an excellent correlation between the hypointense areas of images obtained by *ex vivo* MRI and the areas containing large numbers of SPIO-positive cells as visualized by histochemistry. Even low numbers of SPIO-labeled dendritic cells distributed over a larger area were readily detected by MRI (encircled areas in **Fig. 5b**,**d**). These *ex vivo* MRI and histology findings thus confirm that *in vivo* MRI is a sensitive and accurate technique for monitoring the biodistribution of SPIO-labeled cells.

Further histological evaluation of the lymph nodes beyond the injected node that were detected with autoradiography and MRI showed iron-containing dendritic cells in the paracortex. Large numbers of iron-containing cells were present in the sinuses of the lymph node. These findings indicate that injected dendritic cells entered the lymph nodes via their natural route through the afferent lymph vessels and sinuses (**Fig. 5e**). A significant proportion of the cells penetrated deep into the T-cell areas (**Fig. 5f**) throughout the lymph nodes, whereas no cells were found in the B-cell areas. SPIO-labeled dendritic cells in T-cell areas were often found to be surrounded by rosetting lymphocytes (**Fig. 5g**). The presence of rosettes of slightly enlarged T cells around SPIO-positive dendritic cells is indicative of T-cell activation, a requirement for effective dendritic cell vaccines. The SPIO-labeled cells were negative for the macrophage marker CD68 (**Fig. 5g**), indicating that SPIO-positive cells were indeed injected dendritic cells and not macrophages that had phagocytosed SPIO particles released from dead cells. Moreover, SPIO-containing cells were also positive for the dendritic cell–markers S100 (**Fig. 5h**) and CD83 (data not shown). Thus, SPIO-labeling does not prevent migration of injected dendritic cells to the T-cell area in the lymph node *in vivo*, and injected dendritic cells that migrate into the T-cell areas have productive interactions with resident T cells.

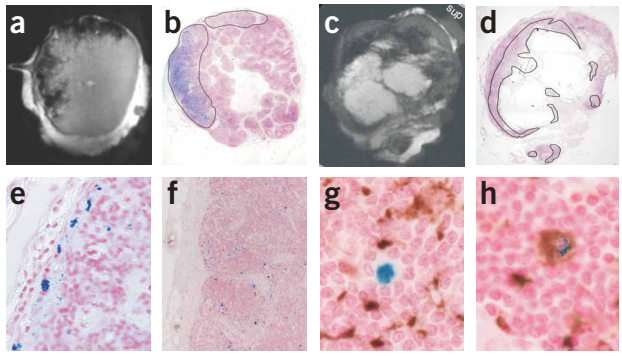

Figure 5 *Ex vivo* magnetic resonance images and correlation with histology. (**a**–**d**) SE magnetic resonance image of the injected lymph node (**a**) and a nearby lymph node (**c**) obtained after resection from patient 1. SPIO-labeled dendritic cells were visualized by Prussian Blue staining in sections from the injected lymph node (**b**) and the nearby lymph node (**d**) at levels comparable to the magnetic resonance images. Areas with (dispersed) SPIO-labeled dendritic cells as detected at higher magnifications are encircled and correlated with the magnetic resonance images. The blue area in **b** that is visible even at low magnification represents the injection site. (**e**–**h**) Magnifications of specific regions of **d**. SPIO-labeled cells were detected in the sinus (**e**) and in T-cell areas (**f**) of the lymph node. (**g**) T cells form rosettes around vaccinated dendritic cells (a representative picture is shown). SPIO-labeled cells are negative for the macrophage marker CD68. (**h**) SPIO-labeled cells were positive for the dendritic cell marker S100. Blue represents SPIO-particles, brown indicates specific immunostaining.

DISCUSSION

In this study, we followed the migration of autologous *ex vivo*-cultured mature dendritic cells after intranodal administration in eight stage-III melanoma patients scheduled for regional lymph node dissection. To the best of our knowledge, there is no previous report of effective tracking of *ex vivo*-labeled therapeutic cells in humans by noninvasive MRI. By co-injecting equal numbers of ^{111}In- and SPIO-labeled cells, we demonstrated that MRI is at least as sensitive as scintigraphic imaging for detecting dendritic cell migration *in vivo*. Moreover, MRI is significantly better than scintigraphic imaging in that delivery of the dendritic cell vaccine to the intended location can be verified and cells can be tracked more accurately.

We labeled dendritic cells in the immature state, following which they were allowed to mature, as immature but not mature dendritic cells are highly phagocytic[21]. This obviated the use and clinical approval of transfection agents, which are now widely applied for efficient intracellular magnetic labeling of nonphagocytic cells in animal models[23]. The phenotypical and functional properties of the SPIO-labeled cells were unaltered as compared with unlabeled cells. Moreover, SPIO-labeled cells that had migrated into lymphoid tissue still expressed the maturation marker CD83, indicating that migrating dendritic cells remained mature and did not return to an immature state.

A major advantage of MRI over scintigraphic imaging is the high-resolution anatomical background contrast, which allows precise anatomical localization of SPIO-labeled cells at the actual injection site and after migration. A major advantage of scintigraphic imaging, however, is the possibility to quantify the amount of cells that have migrated from the injection site. Preferably, both techniques should be combined to obtain both quantitative and qualitative information on migration of therapeutically administered cells. Alternative *in vivo* approaches for noninvasive visualization of adoptively transferred cells, such as bioluminescent imaging or positron emission tomography, have no endogenous background contrast, lack the resolution to

delineate fine anatomical details of tissues and organs or cannot be used clinically (bioluminescent imaging). The combination of both SPIO and radionuclide labeling allows both quantification (scintigraphy) and detailed anatomical localization (MRI) of migrated cells. With these techniques we were able to detect as few as 1.5×10^5 cells *in vivo*, which is in concordance with a previous study in a preclinical porcine model using MRI to visualize injected iron fluorophore particle–labeled mesenchymal stem cells[24] and which is far below the therapeutic range of $\sim 20 \times 10^6$ cells necessary for successful cardiac infarct engraftment[13]. Furthermore, the combination of labeling techniques offers new possibilities to image differentially labeled subsets of cells simultaneously *in vivo* after their injection at one and the same site (for example, dendritic cell subsets or dendritic cells in different activation or maturation stages). This is particularly relevant for further optimization of cell-based anti-cancer therapies. Subsequent autoradiography, (immuno)histology and Prussian blue staining of tissue sections from resected lymph nodes to visualize individual ^{111}In-labeled and SPIO-labeled cells would then offer a further means of validation to track mixed cell populations at the single-cell level.

Interestingly, we found that in only ~50% of the cases were dendritic cells correctly injected into the lymph node, despite ultrasound guidance of the injection needle by a highly experienced radiologist. Subsequent migration could be observed only when dendritic cells were correctly injected into the lymph node, demonstrating the importance for cellular therapy of magnetic resonance verification of accurate delivery. Inadequate delivery may explain why only a limited proportion of patients is responding in ongoing clinical trials of dendritic cell vaccines. We found that MRI was significantly more accurate than scintigraphy for visualizing true dendritic cell–positive lymph nodes. These findings illustrate the power of additional anatomical information, which can also be of value for other fields of biomedical research. For example, the importance of magnetic resonance tracking of cell delivery has been recognized for bone marrow stem cell injections into infarcted myocardium of large animal models[13,24].

MRI proved valuable for monitoring not only the accuracy of the injection but also the migratory capacity of antigen-loaded dendritic cells, as remote lymph nodes containing SPIO-labeled cells could be visualized individually. In contrast to scintigraphy, where a hot spot may represent one or more lymph nodes, MRI can detect all truly positive lymph nodes separately owing to its high spatial resolution and lack of saturation of images. In two patients, individual lymph nodes were missed by scintigraphy because they were located in the same vertical plane as the injection node. With MRI these lymph nodes could be detected separately, allowing correct evaluation of the migratory capacity of SPIO-labeled cells *in vivo*. That these lymph nodes were SPIO positive was confirmed by *ex vivo* MRI and histology.

High-resolution MRI of these targeted lymph nodes *ex vivo* provided detailed information on the three-dimensional biodistribution of small numbers of cells and their migration into the paracortex of the lymph node, the location of the T-cell areas where the dendritic cell–T cell interaction takes place. These findings were confirmed by immunohistology after Prussian blue staining of lymph node sections. Moreover, rosettes of slightly enlarged T cells around injected dendritic cells were present in several patients, demonstrating a functional interplay between SPIO-labeled dendritic cells and T cells. Thus, SPIO-labeling of dendritic cells did not affect the migratory behavior and functionality of the dendritic cells *in vivo*.

In conclusion, this clinical study demonstrates the potential of using MRI for tracking therapeutic cells in patients. Our approach could be easily extended to other clinical applications, including those based on monocyte, granulocyte and lymphocyte trafficking, monitoring of cellular transplants and tissue-restoration therapies based on stem cells and progenitors. The routine imaging protocols we used are readily available on common MRI systems. Therefore, cellular MRI may pave the way for many investigators and clinicians to obtain a more in-depth view of the underlying biodynamics of cellular treatment modalities.

METHODS

Patients. This study included melanoma patients enrolled in an ongoing protocol in which the *in vivo* immune responses of a dendritic cell vaccine are under study (KUN 99-150). Eligibility criteria included stage-III melanoma (according to the 2001 American Joint Committee on Cancer staging system[25]), planned regional lymph node dissection for lymph node metastases, HLA-A2.1 phenotype, melanoma expressing the melanoma-associated antigens gp100 and tyrosinase, and World Health Organization performance status 0 or 1. Prior treatment was allowed, provided that a treatment-free period of at least 4 months was observed and all related toxicity had resolved. Patients with brain metastases, serious concomitant disease or a history of a second malignancy were excluded. The study was approved by our Institutional Review Board, and written informed consent was obtained from all patients. Toxicity was assessed using the National Cancer Institute Common Toxicity Criteria.

In total, 11 stage-III melanoma patients were included, of whom 2 developed clinical overt brain metastases between inclusion and start of treatment and could therefore not be included in the analysis. Of the other nine patients, one had severe claustrophobia precluding *in vivo* MRI, although scintigraphy and *ex vivo* MRI could be obtained. Toxicity was similar to previous dendritic cell vaccination studies[20] and consisted of low-grade fever, mild flu-like symptoms and irritation at the site of injection after the vaccinations in some patients.

Preparation of SPIO- and ^{111}In-labeled dendritic cells. Dendritic cells were generated from adherent peripheral blood mononuclear cells by culturing in the presence of interleukin-4 (500 U/ml) and granulocyte-monocyte colony stimulating factor (800 U/ml) (both Cellgenix). For SPIO-labeling, 200 μg Ferumoxide/ml (Endorem, Laboratoire Guerbet) was added 3 d after the onset of dendritic cell culturing. At day 5, dendritic cells were matured with autologous monocyte-conditioned medium supplemented with prostaglandin E_2 (10 μg/ml, Pharmacia & Upjohn) and 10 ng/ml recombinant tumor necrosis factor-α (Cellgenix) for 48 h, as described previously[26,27]. Dendritic cells were pulsed with the melanoma peptides gp100:154-162, gp100:280-288 tyrosinase 369-376 as described previously[3].

Mature dendritic cells were labeled with ^{111}In-oxine (Tyco Healthcare) in 0.1 M Tris-HCl (pH 7.0) for 15 min at 20 °C as described previously[3,26] resulting in 5 μCi activity per 7.5×10^6 cells. Cells were washed three times with PBS. Radiolabeling efficiency was determined by measuring activity in both the cell pellet and the washing buffer. Iron labeling efficiency was verified by Prussian blue staining. Virtually all cells endocytosed SPIO particles (**Fig. 1**). Total iron content of SPIO-labeled cells was assessed by a Ferrozin-based spectrophotometric assay following acid-digestion of labeled cell samples[11,28]. The iron content was 10–30 pg of iron per cell. Cell viability was determined by Trypan blue staining, showing comparable viability (more than 80%) for unlabeled dendritic cells and ^{111}In and SPIO-labeled dendritic cells (data not shown).

Phenotypic and functional evaluation of dendritic cells. Fluorescence-activated cell sorting (FACS) analysis was performed using a Becton Dickinson FACSCalibur. The following fluorochrome-conjugated monoclonal antibodies were used: anti-HLA class I (W6/32), anti-HLA DR/DP (Q5/13), anti-CD80 (all Becton Dickinson), anti-CD83 (Beckman Coulter), anti-CD86 (Pharmingen), and anti-Chemokine Receptor 7 (kind gift of Martin Lipp). Random *in vitro* migration was tested as described previously[3]. Peptide-specific T-cell stimulatory capacity was tested by coculturing dendritic cells with or without SPIO that were loaded with the gp100:154-162 peptide or an irrelevant peptide with a gp100:154-162 specific T-cell line (dendritic cell:T ratio, 1:5)[22]. After 48 h the cytokines in the supernatant were analyzed with a cytometric bead array for human Th1/Th2 cytokines (BD Biosciences).

Treatment schedule. Within 2 weeks before vaccination a first (preinjection) baseline magnetic resonance scan was performed (see below). At day 7 peripheral blood mononuclear cells were obtained by leukapheresis for dendritic cell culturing. At day 0 patients received a single injection of ^{111}In-labeled dendritic cells (7.5×10^6) mixed with iron oxide–labeled dendritic cells (7.5×10^6, total volume 200 μl) directly into a lymph node of the lymph node region that was to be resected, using a 21 G sterile needle (0.8 × 50 mm, Microlance, Becton Dickinson). Intranodal injections were performed under ultrasound guidance.

One hour after injection the first scintigraphic image (see below) was acquired. At day 2, a second (post-vaccination) magnetic resonance scan was perfomed, followed by a second scintigraphic imaging session, followed by regional lymph node dissection. After surgery, the resected material was again imaged scintigraphically to verify whether all tissue containing radioactivity was indeed removed. Radioactive lymph nodes were dissected from the surgical specimen under guidance of a gamma probe (Europrobe, Eurorad) and then fixed in Unifix (Klinipath). Of these separate lymph nodes, high-resolution *ex vivo* magnetic resonance images were acquired at the end of day 2 and the beginning of day 3. The lymph nodes were sliced and embedded in paraffin at the end of day 3 and sections were cut at day 4 and processed for histology (iron-staining).

As the lymph nodes were to be resected only 2 d after intranodal vaccination, the induction of an immune response might not have been optimal. For this reason patients simultaneously received melanoma peptide-loaded dendritic cells intranodally in a contralateral clinically tumor-free lymph node which was not to be resected. Patients received three more vaccinations at days 14, 28 and 42.

Scintigraphic imaging. *In vivo* and *ex vivo* planar scintigraphic images (256 × 256 matrix, 174 and 247 keV ^{111}In photopeaks with 15% energy window) of the injection depot and corresponding lymph node basin were acquired with a gamma camera (Siemens ECAM) equipped with medium energy collimators, at day 0 and day 2). Migration was quantified by region-of-interest analysis of the individual nodes visualized on the images and expressed as the relative fraction of ^{111}In-labeled dendritic cells that had migrated from the injection depot to following lymph nodes after 2 d.

MRI. Patients were imaged using a 3 T whole body magnetic resonance system (Siemens Magnetom Trio) with a body array radiofrequency coil for signal reception. Magnetic resonance images were obtained with a gradient echo pulse sequence; the signals of three gradient echoes were combined into one T2*-weighted image with an average echo time of 15 ms (flip angle 36°, repetition time (TR) 1,060 ms, total acquisition time ~9 min, 30 slices, resolution 0.50 × 0.50 × 3.50 mm). In addition to T2*-weighted images, which are very sensitive to SPIO-induced magnetic susceptibility effects, SE images at corresponding slice locations were also acquired using a short echo time (TE) of 18 ms (resolution 0.83 × 0.50 × 3.50 mm, TR 2.5 s, total time ~6.5 min) as a reference control to ensure that the decreased signal intensity originated from the magnetic field inhomogeneities caused by SPIO. To keep radiofrequency power deposition within prescribed limits, hyperechoes[29] were used in SE imaging.

Ex vivo MRI of lymph nodes was performed using a 7T MR-spectrometer (Surrey Medical Imaging Systems) equipped with a 20-mm diameter radio frequency (RF) coil. The lymph nodes were placed in a plastic tube filled with Fomblin LC08[10] (Ausimont), to reduce susceptibility artifacts at the tissue-air interface without a background proton signal. Multi-slice gradient-echo imaging was performed at two different echo times (TR = 1,500 ms and TE = 9 and 13 ms, voxel-size = 0.12 × 0.12 × 0.5 millimeters, acquisition time 13 min). Subsequently multi-slice spin-echo imaging was performed at corresponding slice locations and voxel size (TR = 1,000 ms and TE = 15 and 28 ms, acquisition time 8.5 min).

Statistical analysis. Statistical analysis was performed using the Wilcoxon rank sum test for nonparametric distributions for paired and unpaired observations. To test the hypothesis that magnetic resonance is more accurate than scintigraphy, we coded our data for both methods: more lymph nodes visualized by magnetic resonance (MR = +1, scintigrapy = –1); more lymph nodes visualized by scintigraphy (MR = –1, scintigraphy = +1); or equal numbers (MR = scintigraphy = 0). When a hot spot in scintigraphy was qualified as situated outside lymphoid tissue by MRI, this was coded in favor of MRI (MR = +1, scintigraphy = –1). $P < 0.05$ was considered significant.

Iron staining and immunohistochemistry of histopathological sections. Sections (5 μm) of the radioactive resected lymph nodes were stained with Prussian blue to detect SPIO-labeled cells. Slides were stained with 2% potassium hexacyanoferrate (II)-trihydrate in 0.2 M HCl for 15 min and counterstained with 0.05% nuclear fast red in 5% aluminum sulphate.

Immunohistochemistry was performed using antibodies against CD68 (KP1, DAKO), S100 (DAKO) and CD83 (Beckman Coulter). Bound antibody was visualized using powervision (Immunologic). Subsequently the slides were stained using Prussian blue and nuclear fast red.

Note: Supplementary information is available on the Nature Biotechnology website.

ACKNOWLEDGMENTS

Nicole Scharenborg, Mary-lène Brouwer, Annemiek de Boer, Mandy van de Rakt, Mariëlle Philippens, Giulio Gambarota, Andor Veltien, Simon Strijk, Sandra Croockewit, Jos Rijntjes, Emile Koenders, Peter Laverman and Hans Jacobs are acknowledged for their assistance. This work was supported by grants KUN 1999/1950 and 2004/3126 from the Dutch Cancer Society, grant 920-03-250 from the Netherlands Organization for Scientific Research, grants NGT.6719 and NGT.6721 of the Dutch Program for Tissue Engineering, the TIL-foundation, NOTK-foundation and NIH RO1 NS045062. The authors are grateful to Richard A.J. Janssen for his contribution in the initiation of this work.

COMPETING INTERESTS STATEMENT

The authors declare that they have no competing financial interests.

Published online at http://www.nature.com/naturebiotechnology/
Reprints and permissions information is available online at http://npg.nature.com/reprintsandpermissions/

1. Figdor, C.G., de Vries, I.J., Lesterhuis, W.J. & Melief, C.J. Dendritic cell immunotherapy: mapping the way. *Nat. Med.* **10**, 475–480 (2004).
2. Adema, G.J., de Vries, I.J., Punt, C.J. & Figdor, C.G. Migration of dendritic cell based cancer vaccines: *in vivo* veritas? *Curr. Opin. Immunol.* **17**, 170–174 (2005).
3. de Vries, I.J. *et al.* Effective migration of antigen-pulsed dendritic cells to lymph nodes in melanoma patients is determined by their maturation state. *Cancer Res.* **63**, 12–17 (2003).
4. Nair, S. *et al.* Injection of immature dendritic cells into adjuvant-treated skin obviates the need for *ex vivo* maturation. *J. Immunol.* **171**, 6275–6282 (2003).
5. Blocklet, D. *et al.* 111In-oxine and 99mTc-HMPAO labelling of antigen-loaded dendritic cells: *in vivo* imaging and influence on motility and actin content. *Eur. J. Nucl. Med. Mol. Imaging* **30**, 440–447 (2003).
6. Bulte, J.W. & Kraitchman, D.L. Iron oxide MR contrast agents for molecular and cellular imaging. *NMR Biomed.* **17**, 484–499 (2004).
7. Stark, D.D. *et al.* Superparamagnetic iron oxide: clinical application as a contrast agent for MR imaging of the liver. *Radiology* **168**, 297–301 (1988).
8. Weissleder, R. *et al.* Ultrasmall superparamagnetic iron oxide: an intravenous contrast agent for assessing lymph nodes with MR imaging. *Radiology* **175**, 494–498 (1990).
9. Harisinghani, M.G. *et al.* Noninvasive detection of clinically occult lymph-node metastases in prostate cancer. *N. Engl. J. Med.* **348**, 2491–2499 (2003).
10. Weissleder, R. *et al.* Superparamagnetic iron oxide: pharmacokinetics and toxicity. *AJR Am. J. Roentgenol.* **152**, 167–173 (1989).
11. Bulte, J.W. *et al.* Magnetodendrimers allow endosomal magnetic labeling and *in vivo* tracking of stem cells. *Nat. Biotechnol.* **19**, 1141–1147 (2001).
12. Bulte, J.W. *et al.* Neurotransplantation of magnetically labeled oligodendrocyte progenitors: magnetic resonance tracking of cell migration and myelination. *Proc. Natl. Acad. Sci. USA* **96**, 15256–15261 (1999).
13. Kraitchman, D.L. *et al. In vivo* magnetic resonance imaging of mesenchymal stem cells in myocardial infarction. *Circulation* **107**, 2290–2293 (2003).
14. Hoehn, M. *et al.* Monitoring of implanted stem cell migration *in vivo*: a highly resolved *in vivo* magnetic resonance imaging investigation of experimental stroke in rat. *Proc. Natl. Acad. Sci. USA* **99**, 16267–16272 (2002).
15. Kircher, M.F. *et al. In vivo* high resolution three-dimensional imaging of antigen-specific cytotoxic T-lymphocyte trafficking to tumors. *Cancer Res.* **63**, 6838–6846 (2003).
16. Anderson, S.A. *et al.* Noninvasive MR imaging of magnetically labeled stem cells to directly identify neovasculature in a glioma model. *Blood* **105**, 420–425 (2005).
17. Anderson, S.A. *et al.* Magnetic resonance imaging of labeled T-cells in a mouse model of multiple sclerosis. *Ann. Neurol.* **55**, 654–659 (2004).
18. Yeh, T.C., Zhang, W., Ildstad, S.T. & Ho, C. *In vivo* dynamic MRI tracking of rat T-cells labeled with superparamagnetic iron-oxide particles. *Magn. Reson. Med.* **33**, 200–208 (1995).

19. Ahrens, E.T., Feili-Hariri, M., Xu, H., Genove, G. & Morel, P.A. Receptor-mediated endocytosis of iron-oxide particles provides efficient labeling of dendritic cells for *in vivo* MR imaging. *Magn. Reson. Med.* **49**, 1006–1013 (2003).
20. de Vries, I.J. *et al.* Maturation of dendritic cells is a prerequisite for inducing immune responses in advanced melanoma patients. *Clin. Cancer Res.* **9**, 5091–5100 (2003).
21. Banchereau, J. & Steinman, R.M. Dendritic cells and the control of immunity. *Nature* **392**, 245–252 (1998).
22. Bakker, A.B. *et al.* Melanocyte lineage-specific antigen gp100 is recognized by melanoma-derived tumor-infiltrating lymphocytes. *J. Exp. Med.* **179**, 1005–1009 (1994).
23. Bulte, J.W., Arbab, A.S., Douglas, T. & Frank, J.A. Preparation of magnetically labeled cells for cell tracking by magnetic resonance imaging. *Methods Enzymol.* **386**, 275–299 (2004).
24. Hill, J.M. *et al.* Serial cardiac magnetic resonance imaging of injected mesenchymal stem cells. *Circulation* **108**, 1009–1014 (2003).
25. Balch, C.M. *et al.* Final version of the American Joint Committee on Cancer staging system for cutaneous melanoma. *J. Clin. Oncol.* **19**, 3635–3648 (2001).
26. de Vries, I.J. *et al.* Phenotypical and functional characterization of clinical grade dendritic cells. *J. Immunother.* **25**, 429–438 (2002).
27. Thurner, B. *et al.* Vaccination with mage-3A1 peptide-pulsed mature, monocyte-derived dendritic cells expands specific cytotoxic T cells and induces regression of some metastases in advanced stage IV melanoma. *J. Exp. Med.* **190**, 1669–1678 (1999).
28. Bulte, J.W., Miller, G.F., Vymazal, J., Brooks, R.A. & Frank, J.A. Hepatic hemosiderosis in non-human primates: quantification of liver iron using different field strengths. *Magn. Reson. Med.* **37**, 530–536 (1997).
29. Hennig, J. & Scheffler, K. Hyperechoes. *Magn. Reson. Med.* **46**, 6–12 (2001).